

Linköping University Post Print

Origin of the surface recombination centers in ZnO nanorods arrays by X-ray photoelectron spectroscopy

Li-Li Yang, Qingxiang Zhao, Magnus Willander, Xianjie Liu, Mats Fahlman and J H Yang

N.B.: When citing this work, cite the original article.

Original Publication:

Li-Li Yang, Qingxiang Zhao, Magnus Willander, Xianjie Liu, Mats Fahlman and J H Yang, Origin of the surface recombination centers in ZnO nanorods arrays by X-ray photoelectron spectroscopy, 2010, APPLIED SURFACE SCIENCE, (256), 11, 3592-3597.

<http://dx.doi.org/10.1016/j.apsusc.2009.12.160>

Copyright: Elsevier Science B.V., Amsterdam.

<http://www.elsevier.com/>

Postprint available at: Linköping University Electronic Press

<http://urn.kb.se/resolve?urn=urn:nbn:se:liu:diva-54620>

Origin of the surface recombination centers in ZnO nanorods arrays by X-ray photoelectron spectroscopy

L. L. Yang^{1,2*}, Q. X. Zhao¹, M. Willander¹, X. J. Liu³, M. Fahlman³ and J. H. Yang²

1. Department of Science and Technology (ITN), Linköping University, SE-60174 Norrköping, Sweden
2. Institute of Condensed State Physics, Jilin Normal University, Siping, 136000, People's Republic of China
3. Department of Physics, Chemistry and Biology, Linköping University, SE-581 83 Linköping, Sweden

Abstract

The surface composition of as-grown and annealed ZnO nanorods arrays (ZNAs) grown by a two-steps chemical bath deposition method has been investigated by X-ray photoelectron spectroscopy (XPS). XPS confirms the presence of OH bonds and specific chemisorbed oxygen on the surface of ZNAs, as well as H bonds on (10 $\bar{1}$ 0) surfaces which has been first time observed in the XPS spectra. The experimental results indicated that the OH and H bonds play the dominant role in facilitating surface recombination but specific chemisorbed oxygen also likely affect the surface recombination. Annealing can largely remove the OH and H bonds and transform the composition of the other chemisorbed oxygen at the surface to more closely resemble that of high temperature grown ZNAs, all of which suppresses surface recombination according to time-resolved photoluminescence measurements.

Keywords: ZnO nanorods; Optical properties; Surface recombination; X-ray photoelectron spectroscopy

* Author to whom any correspondence should be addressed.
E-mail: Lili.Yang@itn.liu.se

1. Introduction

Zinc oxide (ZnO) as one of the most important semiconductors has attracted significant attention in recent years. Especially, quasi-one-dimensional ZnO nanostructures (e.g. nanorods, nanowires, nanotubes and nanobelts) have been considered highly potential for sensor application such as gas sensor [1-2] and biosensor [3-5], and nanophotonic applications such as nanolasers [6–8], optical waveguides [9–11], and light emitting diodes [12]. However, one of the significant differences between nanostructures and an epilayer is the larger surface-to-volume ratio of the former. This large surface-to-volume ratio can be an advantage for some applications, for example sensor devices [1-5]. However, it can also be a problem in other applications, for example, optoelectronic devices such as light emitting diodes [12] and solar-cell [13-14] devices, since surface states are created within the band gap region either because of surface inhomogeneities like nonstoichiometry or because of the selective adsorption of foreign species in addition to the abrupt termination of lattice periodicity. Such surface states will strongly influence the electronic and optical properties at the semiconductor surfaces and interfaces since the surface recombination rate may become dominating, resulting in a short carrier life time [15-18]. The potential implications of these effects are especially noticeable in the case of nanostructured materials. Therefore, to optimize devices based on ZnO nanostructures, it is necessary to understand the surface recombination mechanisms and explore effective way to control surface states. Furthermore, knowing surface chemical origins in ZnO nanostructures are also essential for their applications in sensor devices based on surface properties. For example, Z. K. Bai et al have reported that the coverage of hydroxyl (OH) groups on the surface of tetrapod-shaped ZnO can inhibit the ethanol adsorption [19-20], i.e. the high ratio of the coverage of OH group can depress the high surface activity of the tetrapod-shaped ZnO sensor and block the

adsorption or reaction sites for the ethanol molecules, which lead to a smaller consumption and sensing signal. Besides, as well known, the attraction or repulsion action between chemical groups on the ZnO surface and detective molecule also influence the sensitivity of ZnO sensor. Therefore, the investigation on the surface recombination and chemical origins of surface recombination centers are significant for the applications of ZnO nanostructures.

As we known, ZnO nanorods are a suitable material for the research on surface recombination due to their large surface to volume ratio. Recently, we successfully controlled the size of well-aligned ZnO nanorod arrays (ZNAs) from 40nm to 150nm with the two-step chemical bath deposition (CBD) method [21, 22], i.e. by first spin coating the substrate with a seed layer of ZnO nanoparticles and then using the CBD growth. And we also investigated in detail the surface recombination of ZNAs with different diameters by time-resolved photoluminescence measurement and revealed that the surface recombination can be strongly suppressed by annealing at 500°C at ambient conditions [23, 24]. We pointed out that the surface recombination maybe originate from the functional groups absorbed by ZNAs surface during the chemical reaction in the solution, which should be related to the elements such as carbon, nitrogen and hydrogen, but we could not identify the origin of the surface recombination due to the limitation of the used characterization techniques [24]. Although some groups have reported the possible functional groups attached in the surface of the ZnO [25-35], so far, there are no investigations which try to build the relationship between the chemical origin and surface recombination centers. On the basis of the discussion in the first paragraph, we believe that the investigation on identifying the chemical origin of surface recombination center is rather important than just revealing the existence of surface recombination in the emission process, because it will open to an effective way to control the surface recombination , utilize

the surface states for sensor application and efficiently enhance the properties of optoelectronic devices based on ZnO nanostructures.

Therefore, in this paper, we utilized X-ray photoelectron spectroscopy (XPS) to investigate the surface composition of as-grown ZNAs and ZNAs annealed in 500°C for 1h in air atmosphere. The results clearly revealed the correlation between the chemical origin and the surface recombination centers of ZNAs grown by CBD method for the first time as far as we know.

2. Experimental

The ZNAs used in this investigation were grown on Si substrates by the CBD method, which includes a two-steps process, i.e. a substrate treatment prior to the CBD growth. The pre-treatment of the substrates, by coating the substrate with a solution of zinc acetate dihydrate ($\text{Zn}(\text{OOCCH}_3)_2 \cdot 2\text{H}_2\text{O}$) dissolved in pure ethanol with concentration of 5mM, was used to control the diameter of ZnO nanorods. In the CBD growth, the aqueous solutions of zinc nitrate hexahydrate [$\text{Zn}(\text{NO}_3)_2 \cdot 6\text{H}_2\text{O}$, 99.9% purity] and methenamine ($\text{C}_6\text{H}_{12}\text{N}_4$, 99.9% purity) were first prepared and mixed together. The concentrations of both were fixed at 0.1M. The pre-treated Si substrates were immersed into the aqueous solution and ZnO was grown at an elevated temperature of 93°C. The more details of controllable preparation process of ZNAs and some other controllable growth conditions can be found elsewhere [21-24]. To guarantee the comparability, a big piece of sample was cut into two parts. One was used as as-grown sample, the other was post-growth thermal treated at 500°C for 1h in air atmosphere and then quenched to room temperature by removal from the oven.

Scanning electron microscopy (SEM) pictures were recorded by using a JEOL JSM-6301F. Transmission electron microscope (TEM) (200keV, JEM-2100HR, Japan) was used to get the high resolution TEM (HRTEM) image and the selected-area

electron diffraction (SAED) pattern of samples. Time-resolved photoluminescence (TRPL) was performed by using an excitation laser line from a frequency tripled sapphire:Ti laser emitting at 266 nm with a 200 fs pulse width and a 80 MHz repetition rate. The luminescence signal is dispersed by a 0.3 m monochromator and time resolved by a streak camera. The spectral resolution is about 1 meV and the time resolution is 7 ps. The measurements were done under weak excitation conditions (0.5 W/cm^2) at 1.8 K. XPS measurements were performed using a Scienta® ESCA200 spectrometer in ultra-high vacuum (UHV) with a base pressure of 10^{-10} mbar. The measurement chamber is equipped with a monochromatic Al ($K\alpha$) X-ray source providing photon with $h\nu=1486.6$ eV. The XPS experimental condition was set so that the full width at half maximum (FWHM) of the clean Au $4f_{7/2}$ line was 0.65 eV. All spectra were measured at a photoelectron take-off angle of 0° (normal emission) and room temperature. The binding energies were obtained referenced to the Fermi level with an error of ± 0.1 eV.

3. Results and discussions

The SEM images of the as-grown and 500°C annealed ZNAs with 90 nm diameters are shown in figure 1(a) and 1(b). In order to show the homogeneity of both samples, only top-view SEM images are shown here. The length of nanorod is about 1 μm . From figure 1(a), it can be seen that the as-grown ZNAs are vertically aligned on the Si (001) substrates. The hexagonally shaped nanorods uniformly cover the entire Si substrate with high density. After 500°C post annealing, the morphology is almost same with the as-grown ZNAs as shown in figure 1(b). The microstructure of the as-grown ZNAs is further characterized by TEM and HRTEM, as shown in figure 1(c) and 1(d). Figure 1(c) shows a low-magnification TEM image, confirming the formation of the one-dimensional ZnO nanorods with 90nm diameter. The inset

SAED pattern further confirms that the as-grown ZNAs grow along the c -axis direction since no splitting of the diffraction spots can be observed. Figure 1(d) displays the typical HRTEM image of as-grown ZNAs. The HRTEM image clearly reveals only the fringes with a lattice spacing of about 0.52 nm (equal to the lattice constant c of ZnO), indicating that the ZnO nanorod is single crystalline in nature and also further confirming that [0001] is the growth direction of the ZnO nanorods.

Figure 2 shows the effect of an annealing on the recombination decay at a relative low temperature of 500 °C. As earlier demonstrated for Si epilayer [36-38], the surface recombination can strongly influence the decay time. The excess minority carriers via the near bandgap recombination exhibit a single exponential decay or a biexponential decay, depending on whether the surface recombination is the major recombination channel or not. Both decay curves exhibited a biexponential decay, which demonstrated the existence of surface recombination [23-24]. To see it clearly, the experimental curves in Fig.2 had been fitted by two exponential decays according to the equation:

$$I(t) = A_S e^{-t/\tau_S} + A_B e^{-t/\tau_B} \quad (1)$$

where $I(t)$ represents the PL intensity as a function of time, while A_S and A_B are the relative weights of the two exponential decays with time constants τ_S and τ_B , respectively. The coloured lines in Fig.2 represent the fitting decay curves according to Eq. (1). The fitting results show that the value of τ_B is the same, 95 ps, for decay curves from both as-grown and 500°C annealed ZNAs. We believe that this time constant τ_B represents an effective “bulk” exciton decay time in these two samples. Then, τ_S is assigned to the time constant which is related to surface recombination. The detailed explanation about the assignments to τ_B and τ_S can be also found in Ref.23, in which theoretical calculated results show a well consistency with these

assignments, especially for τ_s . The value of τ_s is 14 ps and 21 ps for the as-grown and 500°C annealed ZNAs, respectively, which clearly indicates that the decay constant that arises from surface processes increases after annealing, i.e. the post-annealing at 500°C can suppress the surface recombination of ZNAs. For helping us discuss the surface recombination centres later, the decay curve for ZnO nanorods grown at high temperature (HT, 890°C) such as using the VLS growth (named as HT-ZNAs) is also shown in Figure 2. The preparation of HT-ZNAs can be found in our previous work [39]. In this case, the surface recombination can be neglected, and the decay curve follows almost a single exponential decay.

We would like to point out that ZnO nanorods grown by CBD method actually have two kinds of defects, i.e. surface defects and intrinsic defects (also called as deep level defects)[23-24]. To further clearly distinguish the contribution from the surface defects and intrinsic defects, for the prolonged decay time after 500°C annealing, we also investigated the effect of annealing temperature on the optical properties of ZnO nanorods [24]. In Ref. [24], we utilized the Resonant Raman spectroscopy to monitor the change of surface defects and deep level defects in the CBD grown ZnO nanorods under thermal treatment from 500°C to 700°C. By correlating the Raman measurements, PL measurements and time-resolved PL measurements, we proved that the surface defects had a significant contribution to the observed strong Raman intensity of 1LO and 2LO (A_1 -LO mode) in the CBD as-grown samples. The results also clearly indicated that the surface defects played a significant role in the as-grown sample and 500°C annealing treatment can successfully release some part of the surface defects. Therefore, it is not hard to see that the surface recombination centers can be successfully revealed through comparing the surface composition of as-grown and 500°C annealed ZNAs.

XPS was used to investigate the surface composition of as-grown and 500°C annealed ZNAs. Figure 3 shows the XPS survey spectra from as-grown and annealed ZNAs, in which all of the peaks can be only ascribed to Zn, O, and C elements as labeled in Figure 3b [25]. It indicated that there were no other impurities observed in both samples. We would like to mention that, in all the XPS spectra of ZNAs, the binding energies have been calibrated by taking the carbon C1s peak (285.0 eV) as reference.

The deconvolutions of the XPS spectra for the O1s core level line from the as-grown and annealed ZNAs are shown in Figure 4(a) and 4(b), respectively. For all XPS spectra in the paper, the open circles denote the experimental data, red solid line represents the fitting curves and the deconvoluted individual peaks are depicted by green lines. In Figure 4(a), the deconvolutions show the presence of four different O1s peaks in the as-grown ZNAs. The peak centered at 530.35 ± 0.3 eV (O1) is associated to the O^{2-} ion in the wurzite structure surrounded by the Zn atoms with their full complement of nearest-neighbor O^{2-} ions [26-35]. The peak at 531.54 ± 0.3 eV (O2) is attributed to the presence of OH bonds, i.e. ZnO(OH) [28-32]. The binding energy peak at 532.87 ± 0.3 eV (O3) can be ascribed to the specific chemisorbed oxygen, such as $-CO_3$, adsorbed O_2 , or adsorbed H_2O [26-35]. Usually, only these three peaks can be extracted from O1s XPS spectrum. But in our case, we observe another peak located at 528.38 ± 0.3 eV (O4). K. Kotsis and V. Staemmler have reported *ab initio* calculation of the O1s spectra of ZnO and Zn oxo compounds [40], where different binding energy values of O1s were calculated corresponding to different O atoms on the polar O-terminated ZnO(000 $\bar{1}$): adsorption of H atoms (i.e. H-ZnO(000 $\bar{1}$)) with (2 \times 1) and (1 \times 1) surface structure and also the O atoms on the neutral ZnO(10 $\bar{1}$ 0) surface. According to their calculation results, the binding energy

of the O1s peak will be lower than the value of O atoms in bulk ZnO only under two conditions: O atoms in (2×1) H-ZnO $(000\bar{1})$ surface and neutral ZnO $(10\bar{1}0)$ surface. In our case, XPS signal from all different surfaces can be detected for ZNAs grown along the c-axis. However, according to the calculated value in Ref.40, the binding energy of these two peaks is only -0.7 eV and -0.74 eV relative to the oxygen in bulk ZnO, respectively. Even for the experiment result in Ref.41, the energy shift was only -0.90 eV corresponding to the oxygen on the neutral ZnO $(10\bar{1}0)$ surface. While, in our case, the binding energy of O4 peak was about -1.97 eV shift from O1 in Figure 4(a). After comparing our data with Refs 40-41, we believed that it is not possible to have the neutral form of the $(10\bar{1}0)$ surface for ZNAs grown from chemical solution due to the existence of the O2 and O3 features in Figure 4, which imply that the ZnO $(10\bar{1}0)$ surface is attached by either H or OH groups. However, the presence of OH bonds on the surface always increases the binding energy of the O1s feature, in contrast to the measured shift of the O4 feature. Hence the most likely situation in our case is that the ZnO $(10\bar{1}0)$ surface is attached by H bonds. The binding energy of oxygen from H-ZnO $(10\bar{1}0)$ surface can be deduced to be -1.44 eV (from calculation result in Ref.40) lower than that of the oxygen in bulk ZnO, which is much closer to the value of O4 in our experiment. Therefore, we suggested that O4 feature is related to the oxygen from a H-ZnO $(10\bar{1}0)$ surface.

After 500°C annealing, it can be seen from Figure 4 that not only FWHM values of the experimental and fitting curves become much narrower, but also the binding energy and relative intensity of each fitting curve are changed. All these phenomena indicated that the surface of ZNAs had been strongly reconstructed during the annealing process. The relative intensity ratio between O1 and total oxygen (O) calculated from the area of different peaks is 0.16 and 0.31, corresponding to as-

grown and annealed sample respectively. This indicates that the crystallization of ZNAs becomes much better through the annealing process. It is worth to notice that, in comparison with Figure 4(a), the most dramatic change in Figure 4(b) (after annealing) is that the O4 peak totally disappeared and the O2 peak is strongly suppressed. We can thus suggest that O4 and O2 play significant roles in the surface recombination of ZNAs, and we propose that O4 and O2 correspond to the presence of H bonds on $(10\bar{1}0)$ surface and OH on the surface of ZNAs respectively.

We would like to point out here that some oxygen species may not be detectable due to their less concentration than the detection limit of XPS equipment. Although we can not deny their possible contributions to the surface recombination, we can only explain the results which we have observed from the available experimental techniques. We hope our results will stimulate and promote the further investigations in order to definitely conclude the origin of the surface defects which are involved in the recombination.

The participation of O2 in the surface recombination is further supported by the Zn $2p_{3/2}$ XPS spectra. The deconvolutions of the XPS spectra for core level Zn $2p_{3/2}$ from the as-grown and annealed ZNAs are shown in Figure 5(a) and 5(b), respectively. The Zn $2p_{3/2}$ XPS spectrum from as-grown ZNAs was very broad and asymmetric. A good fit to the experimental data only could be obtained when deconvolutions of two Gaussians were used for the spectrum, which indicates that two zinc species exist on the surface of as-grown ZNAs. The observed peak with binding energy of 1021.42 ± 0.3 (Zn1) is associated to Zn species in ZnO [27, 33, 42-43]. The other peak with binding energy of 1022.91 ± 0.3 (Zn2) corresponds to Zn species (1022.73) in ZnO(OH) according to Ref.[44-46]. From Figure 5(a) and 5(b), the relative intensity ratio between Zn2 and total zinc (Zn2+Zn1) can be calculated to be 0.52 and 0.23 corresponding to as-grown and annealed sample respectively, which indicated that the

intensity of Zn2 peak was sharply suppressed after 500°C annealing. This phenomenon further testified that presence of OH bonds as an origin of surface recombination, in excellent agreement with the results from O1s XPS spectra.

We also found in Figure 4(a) and 4(b) that the component O3 ascribed to chemisorbed oxygen can not be removed by annealing even at temperatures as high as 500°C. As mentioned before, O3 is usually ascribed to the specific chemisorbed oxygen, such as $-\text{CO}_3$, adsorbed O_2 or adsorbed H_2O [26-35]. In Figure 4 it can be observed that the binding energy of the O3 peak shifts from 532.87 ± 0.3 eV to 532.28 ± 0.3 eV and the FWHM also decreased from 2.01 eV to 1.60 eV after annealing. The peak position of O3 can vary depending on adsorbant, e.g. from 532.25 eV [29] to 533.21 eV [35], and the exact energy position depended on the relative ratio between the different components involved in O3 peak due to the growth process [26-35]. Therefore, the large shift of the O3 position in Figure 4 indicates a change of the relative contribution to the O3 peak from the different adsorbant components, which might also cause a change in the surface recombination. In order to determine the effects of O3 on the surface recombination, we have to look back on Figure 2. From Figure 2, we can observe that although the decay time for 500°C annealed sample is prolonged compared with the as-grown sample, it still does not totally change into an exponential one like that of the HT-ZNAs, which suggests that although the surface recombination is strongly suppressed by the annealing process, it is still non-negligible in the photoluminescence process. A possible origin for the remnant surface recombination after annealing could thus be O2 that has not totally released and possibly O3 as well.

In order to further investigate the contribution from O3 to the surface recombination, O 1s and Zn $2p_{3/2}$ XPS spectra from HT-ZNAs are shown in Figure 6. From Figure 6(a), we depict the best fit obtained from a deconvolution of two

Gaussians. The two peaks centered at the 530.68 ± 0.3 eV and 532.15 ± 0.3 eV correspond to O1 and O3 respectively. From Figure 6(b), only one component of Zn1 is enough to fit the experiment curve. All these results further testify that the OH and H bonds on the surface are chemical origins of surface recombination in ZNAs grown by CBD method. In addition, from Figure 6(a), it can also be observed that O1 is the dominant part of the whole signal of O1s unlike in Figure 4. The relative intensity ratio of O3/O is only 0.075, in fact, so the effect of O3 can be neglected in the photoluminescence process for the HT-ZNAs. The O3 feature is always the dominant component in the whole signal of O1s in the as-grown and annealed ZNAs grown by CBD method, however, as shown in Figure 4. Hence, we believe that the O3 contribution to the photoluminescence process can not be neglected for such samples and specific chemisorbed oxygen likely contributes to surface recombination. Moreover, in comparison with the annealed sample in Figure 4(b), the binding energy of the O3 feature in HT-ZNAs in Figure 6(a) is shifted to lower energy. Note that the binding energy of O3 in the annealed sample also is shifted to lower energy compared to the as-grown sample as mentioned before. This suggests that the annealing process changes the composition of the chemisorbed oxygen species to something more closely related to the case of HT-ZNAs, which in turn may have a lesser contribution to the surface recombination.

4. Conclusion

In this paper, we have performed an XPS investigation on the surface of as-grown and annealed ZNAs. We found that surface recombination correlates to the presence of OH bonds and specific chemisorbed oxygen on the surface of ZNAs, and H bonds on $(10\bar{1}0)$ surface. The experimental results suggest that OH and H bonds play the dominant role in the surface recombination but specific chemisorbed oxygen also likely affect the surface recombination. Annealing can largely remove the OH

and H bonds and transform the composition of the other chemisorbed oxygen at the surface to more closely resemble that of high temperature grown ZNAs, all of which corresponds to a suppression of surface recombination according to time-resolved photoluminescence measurements. We believe these results can enlighten the other researchers to explore effective ways to suppress the surface recombination, which will prompt the practical application of ZNAs in the future, and the results can also further stimulate theoretical investigation of the surface chemical clusters.

Acknowledgements

The authors would like to acknowledge financial support for this work from the Swedish Research Council (VR) and financial support through Swedish Research Links via VR. L.L. Yang would also like to acknowledge financial support from National Nature Science Foundation of China (NNSFC, No.60878039 and 60778040), program for the development of Science and Technology of Jilin province (Item No. 20090140) and the Eleventh Five-Year Program for Science and Technology of Education Department of Jilin Province (Item No. 20080156).

References:

- [1] H. Zhang, J. B. Wu, C. X. Zhai, N. Du, X. Y. Ma and D. R. Yang, *Nanotechnology* 18 (2007) 455604.
- [2] L. Liao, H. B. Lu, J. C. Li, C. Liu, D. J. Fu and Y. L. Liu, *Appl. Phys. Lett.* 91 (2007) 173110.
- [3] A. Wei, X. W. Sun, J. X. Wang, Y. Lei, X. P. Cai, C. M. Li, Z. L. Dong, W. Huang, *Appl. Phys. Lett.* 89 (2006) 123902.
- [4] A. Umar, M. M. Rahman, S. H. Kim, Y. B. Hahn, *J. Nanoscience and Nanotechnology* 8 (2008) 3216.
- [5] S. Al-Hill, M. Willander, *Nanotechnology* 20 (2009) 175103.
- [6] M. H. Huang, S. Mao, H. Feick, H. Yan, Y. Wu, H. Kind, E. Weber, R. Russo and P. Yang, *Science* 292 (2001) 1897.
- [7] J. C. Johnson, H-J Choi, K. P. Knutsen, R. D. Schaller, P. Yang and R. J. Saykally, *Nat. Mater.* 1 (2002) 106.
- [8] X. Duan, Y. Huang, R. Agarwal and C. M. Lieber, *Nature (London)* 421 (2003) 241.
- [9] M. Law, D. J. Sirbuly, J. C. Johnson, J. Goldberger, R. J. Saykally and P. Yang *Science* 305 (2004) 1269.
- [10] C. J. Barrelet, A. B. Greytak and C. M. Lieber, *Nano Lett.* 4 (2004) 1981.
- [11] A. B. Greytak, C. J. Barrelet, Y. Li and C. M. Lieber, *Appl. Phys. Lett.* 87 (2005) 151103.
- [12] M. Willander, L. L. Yang, A. Wadeasa, S. U. Ali, M. H. Asif, Q. X. Zhao and O. Nur, *J. Mater. Chem.* 19 (2009) 1006.
- [13] Y. Y. Lin, Y. Y. Lee, L.W. Chang, J. J. Wu, C.W. Chen, *Appl. Phys. Lett.* 94 (2009) 063308.
- [14] Z. L. S. Seow, A. S. W. Wong, V. Thavasi, R. Jose, S. Ramakrishna, G. W. Ho, *Nanotechnology* 20 (2009) 045604.

- [15]S. C. Erwin, L. Zu, M. I. Haftel, A. L. Efros, T. A. Kennedy, D. J. Norris, *Nature* 436 (2005) 91.
- [16]P. Zhang, E. Tevaarwerk, B. Park, D. E. Savage, G. K. Celler, I. Knezevic, P. G. Evans, M. A. Eriksson, M. G. Lagally, *Nature* 439 (2006) 703.
- [17]J. J. Boland, *Nature* 439 (2006) 671.
- [18]Q. Wan, T. H. Wang, J. C. Zhao, *Appl. Phys. Lett.* 87 (2005) 083105.
- [19]Z. K. Bai, C. S. Xie, M. L. Hu, S. P. Zhang, D. W. Zeng, *Mater. Science and Engineering B* 149 (2008) 12.
- [20]W. Schmid, N. Bârsan, U. Weimar, *Sens. Actuator B* 89 (2003) 232.
- [21]L. L. Yang, Q. X. Zhao, M. Willander, *J. Alloys and Compounds* 469 (2009) 623.
- [22]L. L. Yang, Q. X. Zhao, M. Willander, J. H. Yang *J. Crystal Growth* 311 (2009) 1046 .
- [23]Q. X. Zhao, L. L. Yang, M. Willander, B. E. Sernelius and P. O. Holtz, *J. Appl. Phys.* 104 (2008) 073526.
- [24]L. L. Yang, Q. X. Zhao, M. Willander, J. H. Yang and I. Ivanov, *J. Appl. Phys.* 105 (2009) 053503.
- [25]Seung Yong Bae, Hyun Chul Choi, Chan Woong Na, and Jeunghee Park, *Appl. Phys. Lett.* 86 (2005) 033102.
- [26]L. J. Meng, C. P. Moreira, and M. P. d. Santos, *Appl. Surf. Sci.* 78 (1994) 57.
- [27]Y. F. Lu, H. Q. Ni, Z. H. Mai, and Z. M. Ren, *J. Appl. Phys.* 88 (2000) 498.
- [28]E. De la Rosa, S. Seplveda-Guzman, B. Reeja-Jayan, A. Torres, P. Salas, N. Elizondo, and M. Jose Yacaman, *J. Phys. Chem. C* 111 (2007) 8489.
- [29]H.H. Wang, S.H. Baek, J.J. Song, J.H Lee and S.W. Lim, *Nanotechnology* 19 (2008) 075607.
- [30]L. J. Meng, C. P. Moreira de Sa and M. P. Dos Santos, *Appl.Surf. Sci.* 78 (1994) 57.

- [31]N. Boulares, K. Guergouri, R. Zouaghi, N. Tabet, A. Lusson, F. Sibieude and C. Monty, *Phys. Status Solidi A* 201–210 (2004) 2319.
- [32]A. Toumiat, S. Achour, A. Harabi, N. Tabet, M. Boumaour and M. Maallemi, *Nanotechnology* 17 (2006) 658.
- [33]M. Chen, X. Wang, Y. H. Yu, Z. L. Pei, X. D. Bai, C. Sun, R. F. Huang, L. S. Wen, *Appl. Surf. Sci.* 158 (2000) 134.
- [34]B. J. Coppa, R. F. Davis, R. J. Nemanich, *Appl. Phys. Lett.* 82 (2003) 400.
- [35]H. H. Wang, C. S. Xie, *Physica E* 40, 2724(2008).
- [36]K. L. Luke and L. J. Cheng, *J. Appl. Phys.* 61, 2282 (1987).
- [37]A. Buczkowski, Z.J. Radzimski, G.A. Rozgonyi and F. Shimura, *J. Appl. Phys.* 69, 6495 (1991).
- [38]K. Thölmann, M. Yamaguchi, A. Yahata and H. Ohashi, *Jpn. J. Appl. Phys.* 32, 1 (1993).
- [39]Q.X. Zhao, P. Klason and M. Willander, *Applied Phys. A* 88 (2007) 27.
- [40]Konstantinos Kotsis and Volker Staemmler, *Phys. Chem. Chem. Phys.* 8 (2006) 1490.
- [41]St.Gil Girol, PhD thesis, Ruhr-Universität, Bochum, 2004.
- [42]N. S. Ramgir, D. J. Late, A. B. Bhise, M. A. More, I. S. Mulla, D. S. Joag, and K. Vijayamohanan, *J. Phys. Chem. B* 110 (2006) 18236.
- [43]C.Y. Leunga, A.B. Djurišić, Y.H. Leung, L. Ding, C.L. Yang, W.K. Ge, J. *Crystal Growth* 290 (2006) 131.
- [44]B. V. Crist, *Handbooks of Monochromatic XPS spectra - Vol.2 - Commercially Pure Binary Oxides*, XPS International, Inc., 1999, PP820.
- [45]R. Umebayashi, N. Akao, N. Hara, K. Sugimoto, *J. Electrochemical Society*, 150 (2003) B295.
- [46]C. Pettenkofer, U. Meier, *Appl. Surf. Sci.* 252 (2005) 1139.

Figure captions:

Figure 1. (a) and (b) SEM images for as-grown and 500°C annealed ZNAs; (c) TEM image of single as-grown ZnO nanorod, the inset is the corresponding SAED pattern; (d) HRTEM of as-grown ZnO nanorod.

Figure 2. Decay curves from as-grown and annealed ZNAs. Decay curve from high-temperature (890°C) as-grown sample was also shown at here for comparison. The decays were measured at 1.8 K. The colour lines are fitted according to Eq. (1).

Figure 3. XPS survey spectra of as-grown ZNAs (a) and annealed ZNAs (b), where the labels indicated the origins of the corresponding peaks.

Figure 4. (a) O1s XPS spectra of as-grown ZNAs where four components (green curves) were used to deconvolute the experimental peak, as labeled by O1, O2, O3 and O4. (b) O1s XPS spectra of ZNAs after 500°C annealing. Only O1, O2 and O3 components were extracted from the experimental curve.

Figure 5. Zn 2p_{3/2} XPS spectra of as-grown ZNAs (a) and annealed ZNAs (b), where two components (green curves) were used to deconvolute the experimental peak, as labeled by Zn1 and Zn2.

Figure 6. (a) O 1s XPS spectra of high temperature (890°C) grown ZNAs, where only O1 and O3 components were extracted from the experimental curve (green curves). (b) Zn 2p_{3/2} XPS spectra of high temperature (890°C) grown ZNAs, one component of Zn1 is enough to fit the experiment curve.

Figure1

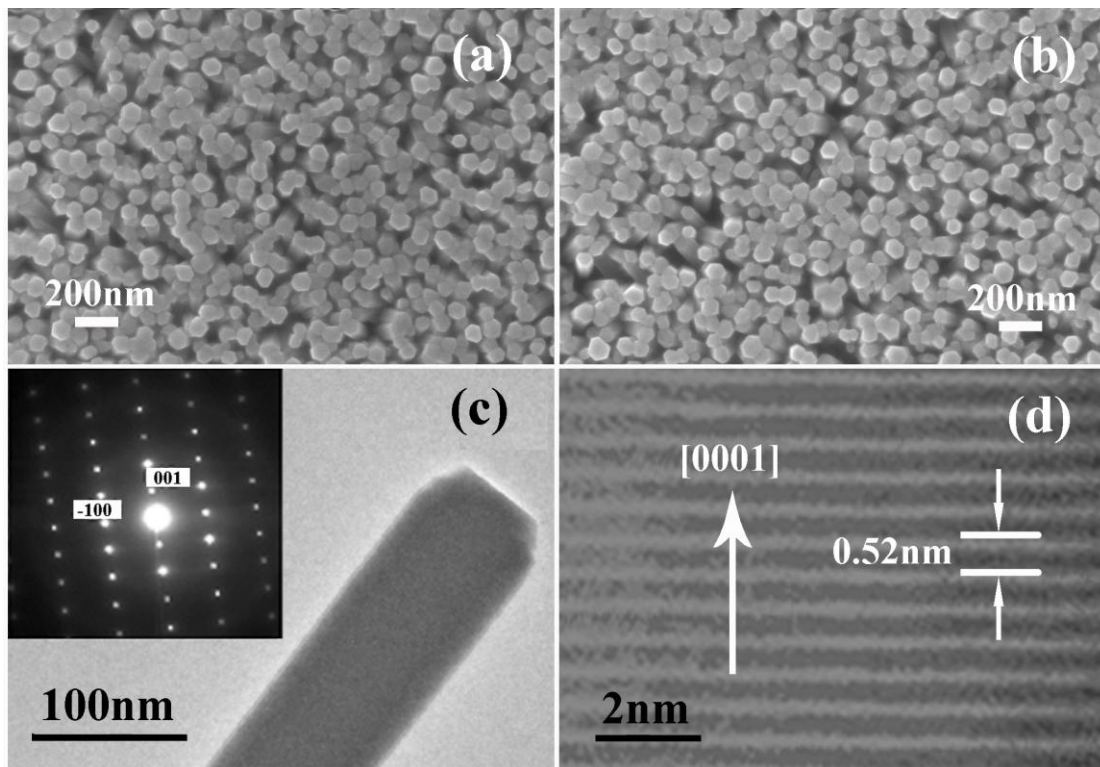


Figure 2

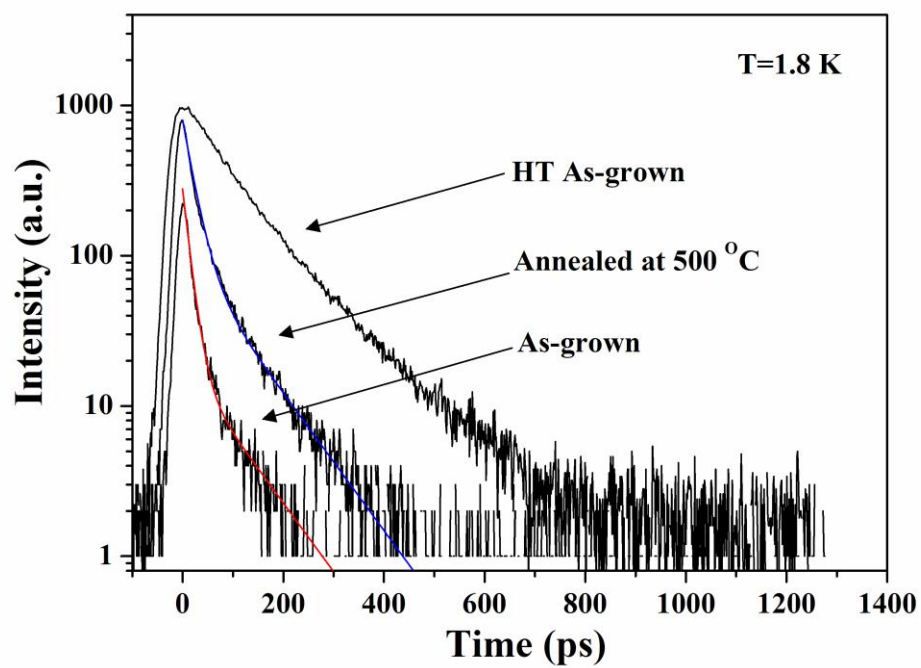


Figure 3

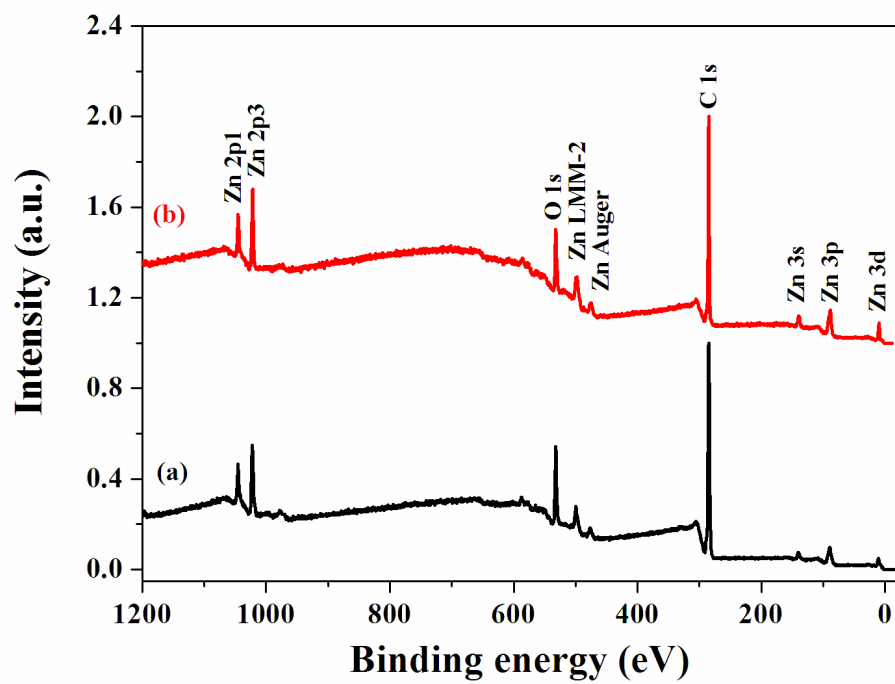


Figure 4

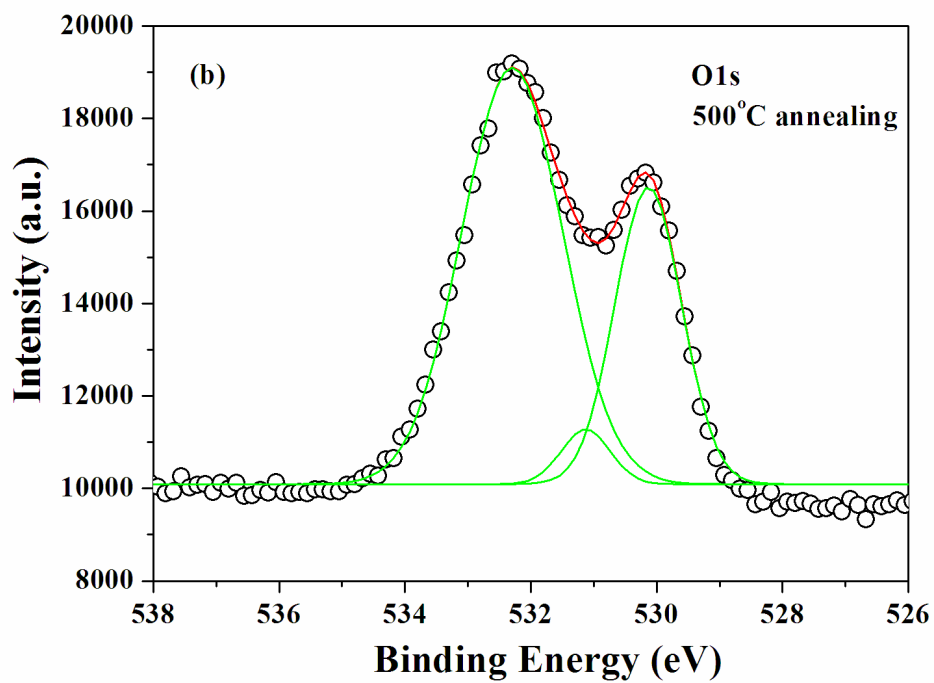
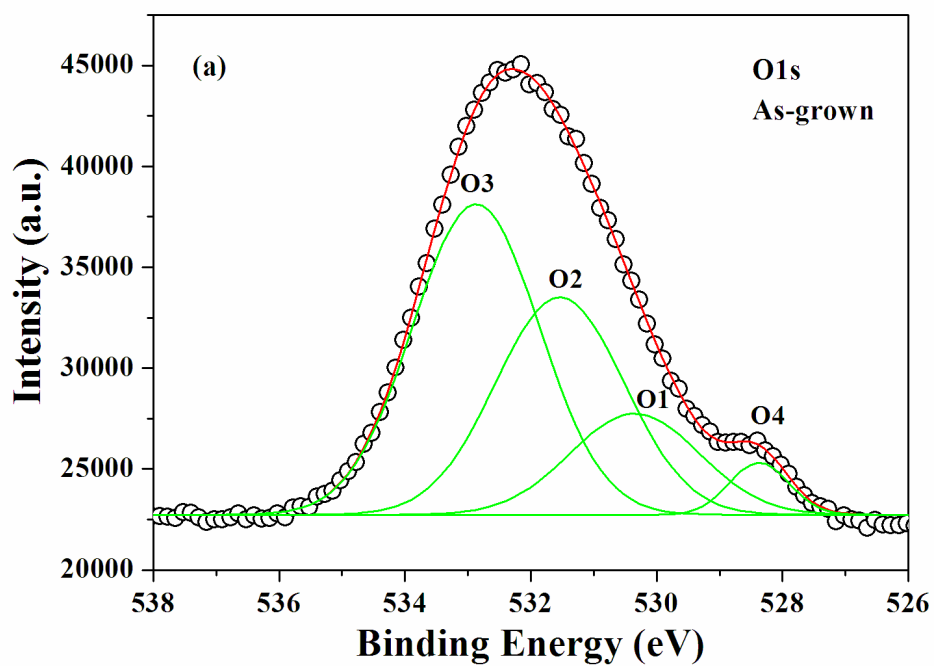


Figure 5

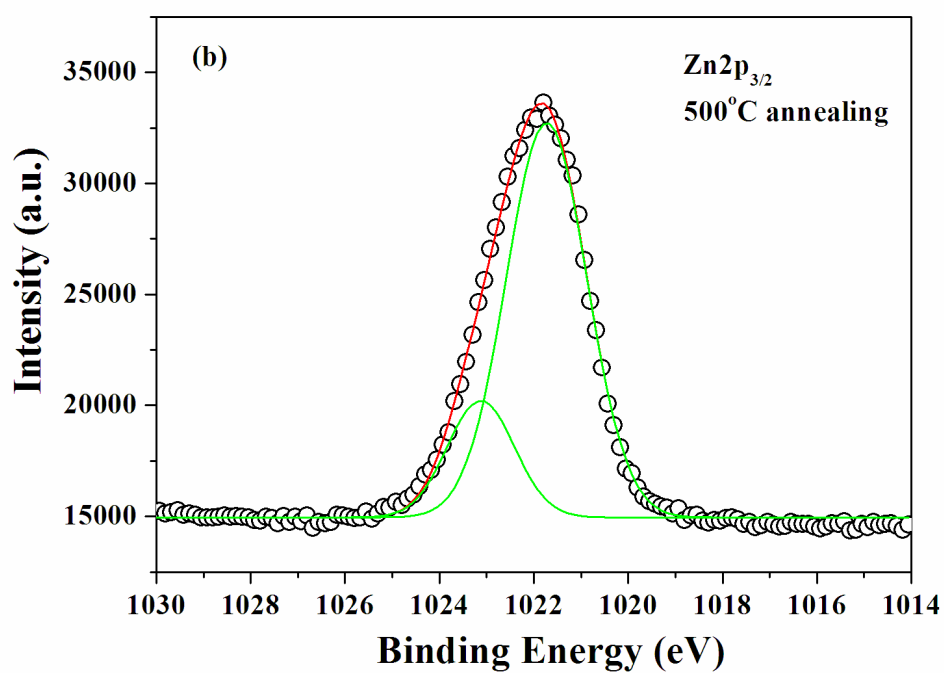
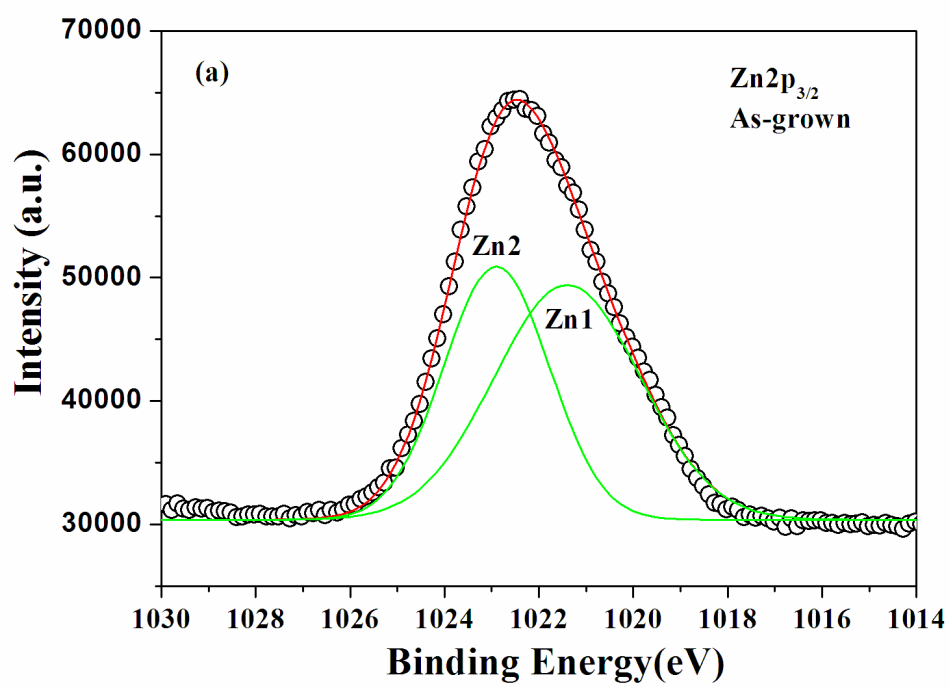


Figure 6

